Robotics and Autonomous Systems 66 (2015) 116–128

Contents lists available at ScienceDirect

Robotics and Autonomous Systems

journal homepage: www.elsevier.com/locate/robot

Towards an affordable mobile analysis platform for pathological walking assessment

V. Bonnet [a,*], C. Azevedo Coste [b,c], L. Lapierre [b], J. Cadic [b], P. Fraisse [b], R. Zapata [b], G. Venture [d], C. Geny [a,e,f]

[a] M2H/EUROMOV, University of Montpellier 1, Montpellier, France
[b] LIRMM, CNRS-University of Montpellier 2, Montpellier, France
[c] INRIA-LIRMM, DEMAR, Montpellier, France
[d] Department of Mechanical Systems Engineering, Tokyo University of Agriculture and Technology, Japan
[e] CHU Montpelier, Neurology Department, France
[f] CHU Montpelier, Internal Medicine and Gerontology Service, France

HIGHLIGHTS

- Mobile robot for clinical assessment of gait.
- Kinect sensor based gait analysis platform.
- Autonomous mobile robot for freezing of gait detection.

ARTICLE INFO

Article history:
Received 27 July 2014
Received in revised form
21 October 2014
Accepted 7 December 2014
Available online 6 January 2015

Keywords:
Rehabilitation
Mobile robot for clinical assessment
Gait analysis
Mobile robot navigation
Kinect sensor

ABSTRACT

This paper proposes an affordable mobile platform for pathological gait analysis. Gait spatio-temporal parameters are of great importance in clinical evaluation but often require expensive equipment and are limited to a small and controlled environment. The proposed system uses state-of-the art robotic tools, in contrast to their original use, for the development of a robust low-cost diagnostic decision-making tool. The mobile system, which is driven by a Kinect sensor, is able to (1) follow a patient at a constant distance on his own defined path, and (2) to estimate the gait spatio-temporal parameters. The Robust Tracking-Learning-Detection algorithm estimates the positions of the targets attached to the trunk and heels of the patient. Real-condition experimental validation including the corridor, occlusion cases, and illumination changes was performed. A gold standard stereophotogrammetric system was also used and showed good tracking of the patient and an accuracy in the stride length estimate of 2%. Finally, preliminary results showed an RMS error that was below 10° in the 3D lower-limb joint angle estimates during walking on a treadmill.

1. Introduction

Evaluation of gait abnormalities is important in the clinical assessment of a patient over time in a large number of medical disorders related to the central nervous system, muscular system, or orthopaedic disabilities, which often affect gait pattern [1]. This evaluation is essential for diagnosis or research purposes and can be performed via a simple visual observation during the medical consultation, i.e., a standard procedure such as the six-minute walking test [2] or a more complete quantitative evaluation in a dedicated laboratory [3]. Devising low-cost and easy-to-use tools to measure the nominal value and the variability of gait spatio-temporal parameters such as step length, gait events [4] or 3D trunk orientation [5] has been the target of extensive studies in or during the last two decades. Indeed, these parameters are representative of the compensatory mechanisms adopted in pathological walking [6]. Some studies have also focused on the detection and identification of a particular gait disorder, such as the freezing of gait [7], which is observed in the majority of people with Parkinson's disease. This freezing of gait (FOG) is the temporary, involuntary inability to move when initiating gait,

* Corresponding author.
E-mail address: bonnet.vincent@gmail.com (V. Bonnet).

http://dx.doi.org/10.1016/j.robot.2014.12.002
0921-8890/

passing through a door, turning, or negotiating an obstacle. The freezing of gait is closely related to the risk of falling [8] and can occur at any time. FOG can occur for very different periods of time and is usually studied using video recordings of the patient's gait [7]. Consequently, trigging protocols of freezing in a confined environment in which video recording, using single or multiple cameras, have been developed [7,8].

Thus, measuring and visualising the patient's walking ability in the clinic but outside of a dedicated motion analysis laboratory for extended periods of time and mobilising the less possible medical staff is one of the goals of bioengineering studies. Although these studies have been performed for decades, most of the existing systems are task- and/or population-specific and/or often require a large investment.

To achieve these purposes, inertial measurement units (IMUs), embedding a 3-axes accelerometer and gyroscope, have gained in popularity due to their low cost and their ease of use [4,5]. Unfortunately, the IMU outputs are subject to a large non-linear drift over time, which jeopardises their time integration [9]. Advanced adaptive filters [5,9] have been used for orientation assessment, but they are task- and population-specific. An assessment of displacement during gait is based on the detection of the zero crossing of the trunk or shank accelerations corresponding to gait events. These events are subsequently used in combination with inverted pendulum models to estimate the step length [10] during straight walking. These biomechanical assumptions can result in very large discrepancies in the case of pathological walking or over prolonged periods of time, and IMU positioning is very sensitive [4,6]. With regard to the detection of freezing events, recent studies have used several IMUs located in the lower limbs for a maximal rate of detection of 80% of positive detection when compared to manual detection performed by clinicians on videotape [7].

Taking into account these considerations, an affordable mobile robot that is able to follow a patient outside the motion analysis laboratory with the purpose of measuring gait spatio-temporal parameters while providing visual video feedback recorded at a constant distance would be a great advantage to clinicians.

The person who is following the patient has two tasks, i.e., the person tracking and the robot navigation or its path generation. Person tracking can use any of the numerous sensor technologies available depending on the context. Measurements from a laser can be used to extract the subject's legs, but other persons or even tables or chair legs can make robust detection difficult [11]. To improve the tracking performance, some authors proposed to merge laser and infrared data [12] or to use an omnidirectional camera [13]. Approaches based on single or multiple cameras to follow a subject have often been proposed [14–17] and have been more recently combined with a depth map [18]. Indeed, a new type of very affordable sensor called light coding has recently become available. The Kinect sensor, which was released by Microsoft®, is a low-cost, compact and lightweight sensor that provides both colour and depth map information. It is being increasingly mainly used in mobile robotics for indoor navigation [19,20] but also for person-following [21–24]. The Kinect sensor represents a significant reduction in robot costs for the replacement of other sensors, including the expensive laser [24]. It is associated with many software that allow for various interactions with humans, but it also allows skeletal tracking or person 3D centroid detection, which is mainly based on silhouette segmentation using the depth map [24]. However, even if several groups have reported using the Kinect sensor person detection ability with mobile robots, few studies have published their results [24]. Moreover, other groups have developed their own algorithms [23,25]. In our application, algorithms such as skeletal tracking will most likely fail because one or several clinicians can be interacting with the patient or they can walk over a short period of time between the robot and the patient. Furthermore, these depth map-based algorithms were originally developed for entertainment purposes and are supposed to be used in an open environment in contrast with our application, which can occur in constrained environments such as a corridor.

To the best of our knowledge, a low-cost mobile gait analysis platform has never been developed and could become very useful for gait clinical assessment. Recently, Ojeda et al. [26] proposed a promising prototype of a mobile platform that yields high accuracy in human gait analysis and subject 3D absolute positioning. However, this approach, which embeds a high-frequency active motion capture system consisting of six cameras and a low-drift gyroscope, requires a large investment and does not provide videotaping. Importantly, no information is provided in their paper concerning the subject-following performance. Indeed, it appears that the mobile platform does not automatically follow the subject while walking and requires an external person to move. Thus, the objectives of this study were to propose a low-cost mobile platform that is able to:

- autonomously follow the patient at a constant distance outside the motion analysis laboratory but still within a clinical environment,
- provide a visual feedback for clinicians to evaluate the freezing of gait,
- accurately estimate the stride length during straight walking and validate this measurement,
- assess the future ability of the proposed system in providing amplitude and temporal information on the lower-limb joint angles.

In this study, the low-cost aspect, the ease of use and the assessment of reliability in spatio-temporal measurements are of great importance to allow such devices to be widely used among the clinician community. The novelty of the approach is the development of algorithms that allow the ability to autonomously follow a patient while accurately estimating stride length during straight walking, including a visual feedback of gait. In addition to a new, parcimonial and robust path generation method from human motion estimated from a noisy low-cost sensor, the use of state-of-the art mobile robotics path planning, path recovery and visual servoing approaches has been validated in a different context compared to previous methods. Finally, a new method to estimate human stride length from a mobile platform has been developed and has proven to be robust to noise and odometry inaccuracy.

Consequently, this paper is organised as follows: Section 2 presents a low-cost platform and its hardware components. Tracking of the person and the associated visual servoing and path construction and following are discussed in Section 3. The strategy used to estimate the stride length is detailed in Section 4. The last section discusses the experimental validation in the real-clinical assessment condition using a stereophotogrammetric system as a gold standard measurement tool.

2. Hardware

The low-cost mobile gait analysis platform was implemented on an experimental mobile robot shown in Fig. 1. The mobile robot is based on a generic differential drive mobile platform with two propulsive wheels and one castor wheel (Pioneer 3DX robotic platform). A Kinect sensor, which provides colour and depth images with 640×480 resolution, was mounted horizontally on a mast at a tunable height that was selected to be approximately at the subject's pelvis height. Under ideal conditions, the resolution of the depth information can be approximately 3 mm [27]. In general, the further the Kinect sensor is from the object to measure, the less accurate the depth map obtained. To measure the trunk and heel positions with the best accuracy and to account for the

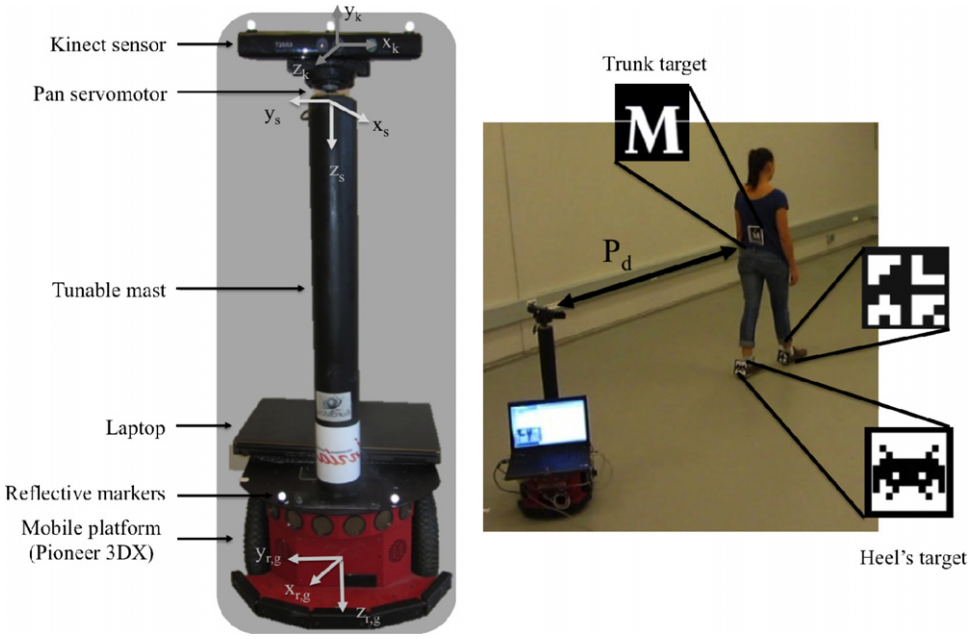

Fig. 1. Detail of the proposed system and experimental setup.

vertical field of view of the Kinect sensor (48.6°), the desired distance P_d between the person and the robot (see Fig. 1) is chosen to be between 1.2 and 1.7 m depending on the subject's height.

The maximal sample rate of the Kinect sensor is 30 Hz for both the colour and depth cameras; unfortunately, this frequency rate is not constant. Consequently, all Kinect sensors and robot data were time stamped. Thus, all data were interpolated using a first-order approximation to a fixed sample rate of 30 Hz.

The absolute tilt orientation of the Kinect sensor, which is mechanically kept fixed during all experiments, was computed using the accelerometer embedded in the Kinect sensor. A pan mechanism used to decouple the patient tracking and robot motion has a range of 180° and was initialised to a value of zero.

Person following began by the selection of the target of interest located on the lower trunk. The chosen target, the logo of Montpellier city, was attached to the body segment using double-sided tape. The subject 3D position, P_g, in the global system of reference needs to be estimated. The global system of reference is defined as the frame attached to the robot in the first sample. This estimate can be obtained using available data from the Kinect, i.e., in the Kinect local frame, the current pan servo angle, and the robot local odometry. Using these quantities, the so-called direct kinematic can be used to obtain the subject 3D position:

$$P_g(t) = {}^{g}T_r(\psi(t), X_r(t), Y_r(t)) \; {}^{r}T_s \; {}^{s}T_k(\theta_s(t)) P_k(t) \quad (1)$$

where P_k is the 3D position vector of the subject in the Kinect sensor frames. The transformation matrices, ${}^{g}T_r$, ${}^{r}T_s$, ${}^{s}T_k$, account for rotations and rigid transformations from the robot to the global frame, from the pan servo to the robot, and from the Kinect sensor to the pan servo frame, respectively. $(\psi, X_r Y_r)$ are the instantaneous robot orientation and linear displacement following the X and Y initial axes. θ_s is the instantaneous pan servomotor supporting the Kinect sensor. An overview of the system software modules that will be detailed in the next sections is shown in Fig. 2. The system consists of three main parts. The visual-servoing indicated in blue (Fig. 2) displays an estimate of the 3D patient position in the global system of reference. The green colour represents the definition of the robot trajectory and path from the 3D patient position. Finally, an off-line software module, which is highlighted in red in Fig. 2, is used to estimate the stride length.

3. Patient tracking algorithms

3.1. Visual servoing

This section describes the visual-servoing part highlighted in blue in Fig. 2. Both the colour and depth images from the Kinect sensor are calibrated to reduce distortion and to obtain the intrinsic parameters to accurately map the depth and colour pixels. To achieve this purpose, the toolbox developed by Herrera et al. [28] was used to obtain the Kinect sensor-specific parameters.

Next, we obtained reliable depth and colour maps to track the subject 3D position. Generally, to detect a human using a Kinect sensor, the first approach is to use background subtraction methods. Unfortunately, this type of approach is not appropriate in our situation because the background is continuously changing. As stated in the Introduction, the algorithms provided by Microsoft [29] for automatic subject detection and tracking based on the depth map were tested. However, in our application, the robot was mainly moving in a narrow corridor and the Kinect pan rotation could be very fast during the turning parts. Because the clinicians could surround and/or be in contact with the subject, these algorithms were not able to satisfactorily detect and track the subject. The subject's clothes, i.e., colour and texture, were also used in the human following task [16,17]. Despite good robustness, such approaches were not very accurate due to the size of the pattern of interest. A simple 3D centroid trajectory as a variable to locate the subject appears to be more suitable. In addition, the lower trunk area, which is closely related to the subject's centre of mass during walking, is a variable of interest in clinical applications, and its assessment has been the objective of numerous studies [5,9]. For these reasons, a target was attached to the lower trunk of the subject (see Fig. 1). The chosen target is a unique pattern and is similar to the patterns used in enhanced reality applications. Due to the specificity of the pattern, its tracking is easier and the risk of a mistake with other elements of the environment was reduced in contrast, for example, to the red patch associated with a blob expansion method.

Because the robot needs to follow a target attached to an oscillating human segment and in various environments such as a corridor or bay windows, robustness to illumination, occlusion

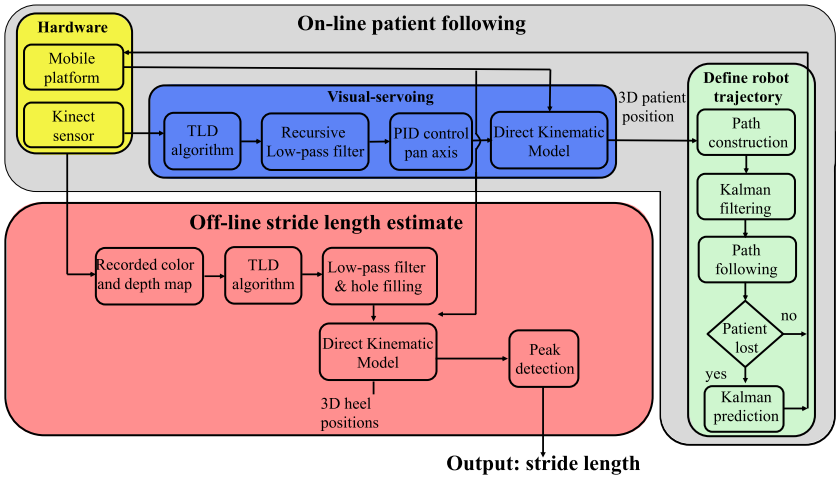

Fig. 2. Overview of the system software modules proposed for patient following and for the stride length estimate.

and scale and orientation change are challenging. In addition, as presented by Papadourakis and Argyros [30], the majority of the short-term object tracking algorithms in the literature assume no complete occlusion or disappearance of the tracked object, as is the case in our application. Recently, Kalal et al. [31] proposed the so-called Tracking Learning Detection (TLD) framework, which is designed for long-term tracking of unknown patterns in a video stream. This framework, which is based on learning frame-by-frame, proposes to re-initialise the tracker after a complete occlusion. The first element of the TLD framework is the short-term tracker, which estimates the object's motion between consecutive frames under the assumption that the motion between consecutive frames is limited. The tracking component of the TLD is based on the median-flow tracker [31], which estimates displacements of a number of points using a Lucas–Kanade tracker [32], which is contained in a bounding box used to represent the object. As previously stated, the tracker will never recover if the object disappears from the image. To address this issue, a detector based on the cascaded architecture [33] will treat each frame independently and will perform a complete scanning of the image to localise all appearances that have been observed and learned in the past. Finally, a dedicated machine-learning component, which has been described in detail and analysed by Kalal et al. [31], observed the performances of the tracker and detector and estimates their errors to generate training examples. These examples will be used to avoid these errors in the future. The learning component is based on two "experts", which account for real and false positives independently. The combination of the results of these two experts will provide a more suitable database that can be used for the detector. Importantly, the available version does not perform well on articulate objects, such as the human body.

Once the trunk pattern is located in the colour image, the associated 3D position in the Kinect sensor frame is calculated. The angle α, which is defined between the origin of the Kinect sensor frame (see Fig. 1) and the subject position, is calculated from these data as follows:

$$\alpha = \operatorname{asin}\left(\frac{P_{kx}}{|P|}\right) \tag{2}$$

where P_{kx} and $|P|$ are the position of the subject along the x-axis and the absolute distance of the person in the Kinect sensor frame, respectively.

The angle α was filtered using a recursive low-pass filter that accounts for the Kinect sensor's variable delay [33]. A control law of the pan axis was developed to point the Kinect sensor towards the tracked subject. A Proportional-Integral-Derivative controller is used to control the pan servomotor (see Fig. 1) with $\alpha_d = 0$.

3.2. Path construction

This section discusses the first two blocks of the system component that defines the robot trajectory highlighted in green in Fig. 2. Navigation of the mobile robot in a real environment while following a human target can be performed in very different ways [24]. In this context, the human target will be a patient suffering from a pathological disorder that affects his gait velocity, so the patient's perception of the environment and thus the ability to avoid obstacles or walk in very narrow environments is affected. Usually, walking tests are performed in motion analysis laboratories [1,3], which reduce the number of steps that can be analysed, or in a long straight corridor to observe the walking phases at a constant velocity [2]. For these reasons, it is reasonable to suppose that the environment in which the walking task will occur will be relatively free of obstacles and consists of long straight lines. To reduce the cost of the mobile platform, we selected to not use any external sensor, such as laser range or ultrasound sonar, for obstacle avoidance but to simply suppose that, by definition, the path followed by the patient is free of obstacles. Obviously, if needed, obstacle avoidance functionality can be added in future versions.

Nevertheless, due to the specific dynamics of the mobile robot, mainly the effect of its mass and its inertia in decelerating while turning, and of the measurement noise in the Kinect sensor, it is not appropriate to update the path at each sample of time without filtering. Indeed, taking into account all of the measurements will result in numerous small variations in the path that the robot will have to follow. The error and delay in the following path will accumulate and may result in erratic behaviour. This challenge was addressed by creating a circular area around the first subject position determined in the global system of reference, as represented in Fig. 3. The diameter of this circular area was set based on field experiments to $C_D = 0.5$ m. A new point in the path, i.e., a new circular area, will be created when three consecutive measurements are obtained outside of this initial circular area. This allows for a dramatic reduction in the number of points in the path. The obtained path is then filtered using a discrete time, linear state-space Kalman filter in which the state is expected to be constant. In this case, the retained Kalman filter acts as a low-pass filter to reduce the Kinect sensor noise effect but with a reduced offset.

The patient position in the global system R_G of reference was estimated, even if it is not always taken into account in the path construction, at each sample time using the Kinect sensor and the robot local odometry information. The coordinates of the patient position in the colour image provided by the TLD algorithm were

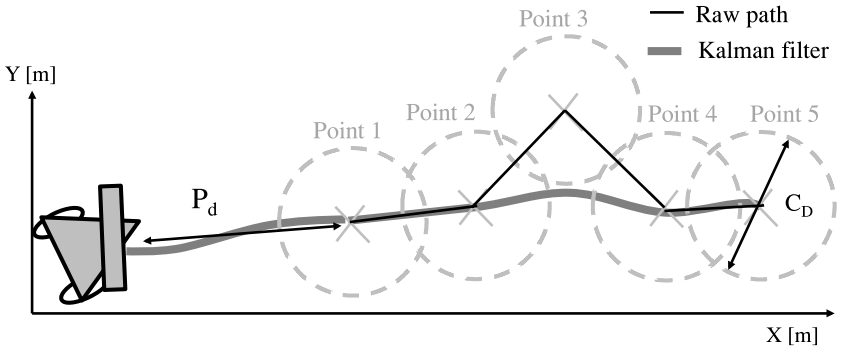

Fig. 3. Principle of path construction using the circular area and Kalman filtering.

used in combination with the calibrated depth map to obtain the 3D patient position in the Kinect sensor system of the reference R_K. The patient position was then expressed in the R_G frame using transformation matrices (see Section 2) accounting for the Kinect sensor pan angle and current robot absolute pose ψ.

A second Kalman filter, based on a double integrator, assuming a constant speed of the subject, was implemented in the case of patient loss. The Kalman filter predicts the 2D location of the subject based on previous states, and if the subject is detected at the current time step, then its location is used to correct the states. On the basis of this prediction, the robot will continue to follow the path for a maximal time of 2 s. This value, which is derived from field experiments, appears to be a good compromise between safety and robot autonomy and is, for instance, sufficient for door passing or occlusion due to person passing between the robot and patient. Indeed, the maximal expected velocity of the patient would be approximately 1 m s^{-1}.

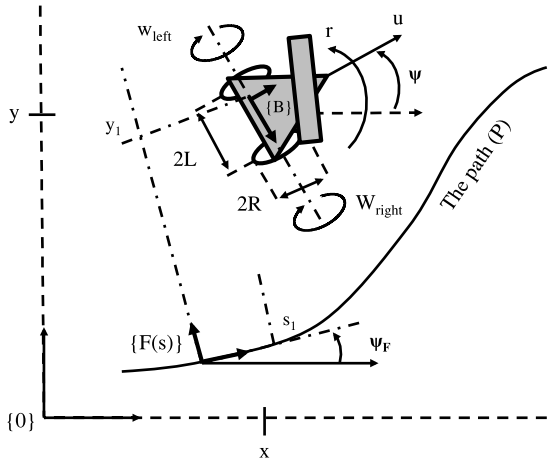

Fig. 4. Path following problem formulation.

3.3. Path following

This section concerns the two last blocks of the system part defining the robot trajectory highlighted in green in the system overview in Fig. 2. The solution to the problem of path following admits an intuitive explanation: a path following controller should look at (i) the distance from the vehicle to the path and (ii) the angle between the vehicle velocity vector and the tangent to the path and should reduce both to zero. This motivates the development of the kinematic model of the vehicle in terms of a Serret–Frenet frame $\{F\}$ that moves along the path; $\{F\}$ plays the role of the body axis of a *path following target*, located on the path according to the curvilinear abscissa s, which should be tracked by the vehicle. Using this set-up, the abovementioned distance and angle become the coordinates of the error space $(s_1,\ y_1,\ \theta)$, where the control problem is formulated and solved, according to Fig. 4, and is expressed in Eq. (3).

$$\begin{aligned} \dot{\boldsymbol{s}}_{\mathbf{1}} &= -\dot{\boldsymbol{s}} \cdot (\mathbf{1} - \boldsymbol{c} \cdot \boldsymbol{y}_{\mathbf{1}}) + \boldsymbol{u} \cdot \mathbf{cos}(\boldsymbol{\theta}) \\ \dot{y_1} &= -c \cdot \dot{s} \cdot s_1 + u \cdot \sin(\theta) \\ \omega &= r - c \cdot \dot{s} \end{aligned} \tag{3}$$

where c designates the local curvature of the path in s, and θ is the relative angle between the path and the robot, i.e., $\theta = \psi - \psi_F$ and $\omega = \dot{\theta}$. For a detailed derivation, the reader is invited to refer to Lapierre et al. [34]. The system can be velocity controlled, i.e., the control inputs are $(u,\ r)$, where u is the forward velocity and r the rotational one. Equivalently, the control expression can consider the wheel velocities as control inputs, i.e., $(w_{left}\, w_{right})$, with the following relationship:

$$\begin{aligned} w_{left} &= \frac{1}{R} \cdot (u - L \cdot r) \\ w_{right} &= \frac{1}{R} \cdot (u + L \cdot r) \end{aligned} \tag{4}$$

where R is the wheel radius and L is the half distance between the wheels along their axis. Using this framework, the path following solution is to design a kinematic control law, in terms of $(w_{left}\, w_{right},\ \dot{s})$, which asymptotically and uniformly drives the unicycle robot to the path, with a desired arbitrary forward velocity profile u_d. This approach decouples the heading control from the forward velocity, differing from the trajectory control approach where both the kinematic variables u and r are coupled. This advantage will be used in the sequel to design an explicit control for the forward velocity u to warrant the respect of a desired distance between the system and patient.

We introduce the approach angle $\delta = -\theta_A \cdot \tanh(k_\delta \cdot y1)$, where k_δ is an arbitrary positive gain, and θ_A defines the asymptotic desired approach, which defines the approach angle when $|y_1|$ is large. Traditionally, $\theta_A = \pi/2$, which indicates that the system is driven to the path with a relative incidence of $\pi/2$, i.e., perpendicular to the path. Next, as shown in Lapierre et al. [34], the following control law solves the path following problem:

$$\begin{aligned} \dot{s} &= u \cdot \cos\theta + K_s \cdot s_1 \\ r_{PF} &= \dot{\delta} - K_1 \cdot (\theta - \delta) + c \cdot \dot{s} \end{aligned} \tag{5}$$

where K_1 and K_s are arbitrary positive gains, and u_d is an arbitrarily chosen positive. The reader is invited to read Lapierre et al. [34] for the complete proof, extension to dynamics and robustness. The forward velocity control has to insure that a desired distance between the system and the patient is maintained, extending the previous path following the solution to trajectory tracking [35]. The current distance between the robot and patient is estimated using the Kinect sensor measurement P, as defined in Fig. 1. The convergence of P to P_d is performed using a Proportional-Integral controller.

4. Stride length estimate

This section concerns the off-line estimate of stride length, which is represented in red colour in Fig. 2. In this section, the recorded raw data from the Kinect sensor, servo pan angle and robot local odometry were used to track two unique targets in the global system of reference, size 0.08 × 0.08 m, which is located on the subject's heels as represented in Fig. 1. The TLD algorithm was run off-line using the recorded colour image to track these two targets. Matching with the calibrated depth map was subsequently performed to obtain heel 3D positions in the Kinect sensor frame. For depth images that are very noisy, erosion and dilation [36] were used to reduce noise, and a hole filling strategy was used in the case of missing data. This procedure simply requires calculating the mean value of the pixels surrounding the hole. In case of an absence of data in the area of interest, missing data were labelled as such. These positions were then calculated in the global system of reference using the direct kinematic model of the robot. This finding indicates that in addition to the Kinect sensor measurement, error-prone local odometry of the mobile platform is required. However, because the stride length analysis is relative from one stride to another, which occurs in a straight line, and the duration is approximately one second, this error can be neglected. The eventual gaps created by the labelled missing data were automatically filled using a classical cubic spline interpolation method [37].

The automatic stride length estimation is crucial in the objective of optimising the time of the clinicians. In motion analysis, literature stride length estimation is generally performed using peak detection methods [4,6], which mainly require an accurate detection of heel strike events. In our application, due to the flickering noise and the maximal frame rate of 30 Hz of the Kinect sensor, it is difficult to accurately identify heel strike events. Consequently, the mean value position of the foot during stance, which is not supposed to vary, was used instead of heel strike events. First, the heel positions in the subject plane were calculated using principal component analysis to determine the Antero-Posterior axis (AP), i.e., the forward progression axis of the subject. Second, as illustrated in Fig. 5(a), the derivative of the foot displacement along the AP axis was used to detect the maximal signal peaks corresponding to the change in direction during the foot flying phase. The index of all points present consecutive to these peaks and that are below an experimentally chosen threshold, set to $T_h = 0.15$ m s^{-1}, were selected because they correspond to the foot stance. The position of the heel was then calculated by grouping and averaging the corresponding values of the foot displacement along the AP axis as illustrated in Fig. 5(b).

5. Lower limb joint angles estimate

Lower limb joint angles are of interest in the case of a biomechanical analysis of human gait [1]. At a more macroscopic level, lower-limb joint coordination during gait can be used to quantify the deficit and gait adaptation of different populations, such as an elderly [38] or Parkinsonian patient [39,40]. For the latter population, motion analysis techniques have been used to determine the effect of the levodopa [40] drug on the lower-limb joint range of motion. In this context, it is important to provide accurate information of the lower-limb joint angles.

As represented in Fig. 6, 3D trajectory of the heels and trunk can be assessed easily using the proposed system. These trajectories represent five steps obtained during a straight walking condition.

Starting from the 3D world marker trajectories, an offline inverse kinematics module was developed to estimate the joint angles of a six degrees-of-freedom floating base lower-limb model

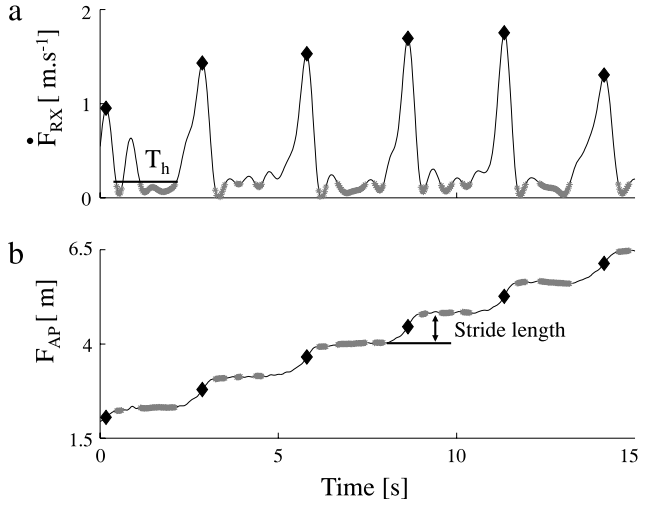

Fig. 5. Identification of the stride length based on the estimated foot displacement along the AP axis (F_{AP}). (a) The derivative of the FAP was used to detect the maximal peaks and points corresponding to the foot stance between two consecutive maximal peaks selected if below threshold T_h.

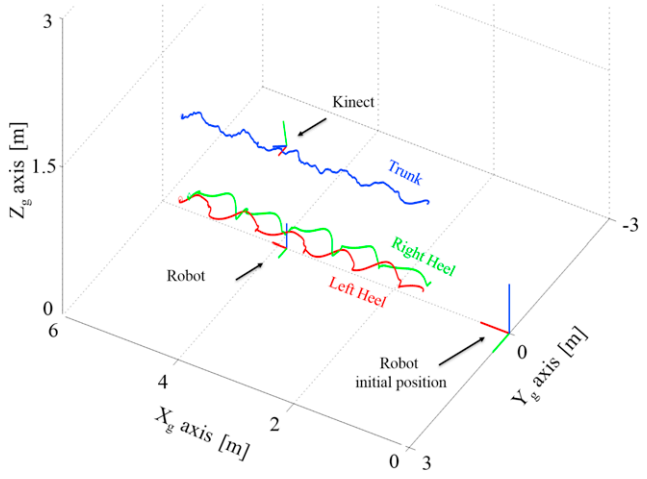

Fig. 6. Representative results depicting the ability of the proposed system to estimate the 3D position of the patient trunk (blue line), right heel (green line), and left heel (red line). (For interpretation of the references to colour in this figure legend, the reader is referred to the web version of this article.)

(see Fig. 7). The following joint angles were estimated: adduction/abduction (q_1, q_4) of and flexion/extension (q_2, q_5) of the hips and flexion/extension of the knees (q_3, q_6) because they are the most often reported in gait analyses [1]. The basis of the model is located at the centre of the pelvis marker. Consequently, the left (P_{Lmes}) and right (P_{Rmes}) foot 3D positions were calculated in the lower-limb system of reference, which was attached to the pelvis marker via a rigid transformation. This has the advantage, similarly to the stride length estimate, of avoiding drift in the robot's odometry, which occurs over an extended period of time.

The inverse kinematics module is based on the so-called global optimisation method [41]. The principle of this inverse kinematic module is to identify the joint angle vector $\boldsymbol{q}$ that minimises the total least-squares difference, J, between the measured positions of the markers and their estimates in the lower-limb model system of reference. In the literature, this problem is often solved at each time sample. Due to the noise in the Kinect sensor, the following cost function is solved for all of the collected samples of time N:

$$\mathrm{J} = \frac{1}{N}\sum_{i=1}^{N}(\boldsymbol{P_{Lmes}}(i) - \boldsymbol{P_{Rest}}(\boldsymbol{q}(i)))^2 + (\boldsymbol{P_{Rmes}}(i) - \boldsymbol{P_{Rest}}(\boldsymbol{q}(i)))^2 \quad (6)$$

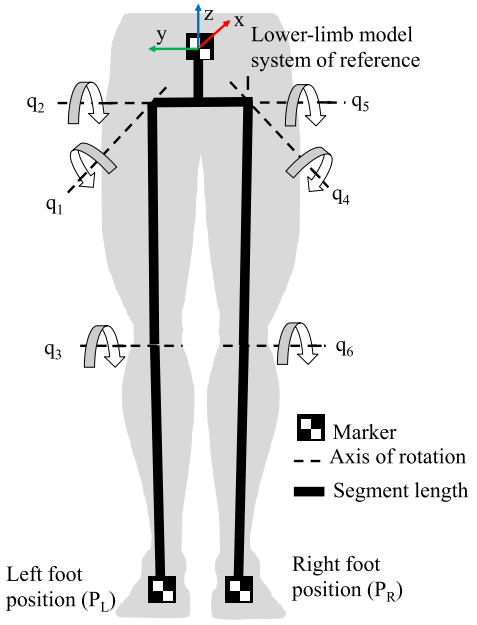

Fig. 7. Six-degrees-of-freedom model of the locomotor system. The subject is viewed from the back.

where $\boldsymbol{P_{Rest}}$ and $\boldsymbol{P_{Lest}}$ are the right and left estimated foot positions from the direct forward kinematic model. The direct kinematic forward is a function of the joint angles and of the segment lengths that were measured a priori on the subject.

Biomechanical constraints, which state that the joint angle limitations and joint velocities should be within their physiological boundaries, were used to reduce the search space and to provide a feasible solution.

$$q_{min} \leq q \leq q_{max}$$
$$\dot{q}_{min} \leq \dot{q} \leq \dot{q}_{max} \tag{7}$$

where $q_{min}, q_{max}, \dot{q}_{min}, \dot{q}_{max}$ and are the minimal and maximal boundaries of the joint angles and joint velocities, respectively.

This optimisation problem was solved numerically using a gradient-based non-linear constrained sequential quadratic programming method [42].

6. Experimental validations

Two sessions of experiments were performed with young healthy subjects as described in Fig. 8. The first experiment focused on the system tracking, stride length accuracy evaluation and joint angle estimate using a stereophotogrammeteric system, which is considered to be a gold standard evaluation tool. The second set focused on the adaptive person following algorithm in a real environment.

6.1. Performance analysis using the gold standard method

One volunteer (1.70 m, 65 kg, 27 years) participated in the double performance evaluation of (i) the patient tracking and (ii) evaluation of the accuracy in the stride length estimate. Two retro-reflective markers were located on each subject's heels and on his trunk, and four markers were used to locate the centre of the mobile robot as indicated in Fig. 1. The 3D trajectories of the markers were recorded using an eight-camera stereophotogrammetric system (MX-13, VICON©) sampled at 100 Hz. The capture volume was approximately 5 × 3 m with 1 mm accuracy in estimating the individual marker locations.

(i) In the first experiment, the person was instructed to walk naturally around the capture volume during 180 s. The desired norm of the distance between the subject and robot was set to $P_d = 1.550$ m to visualise the heels and trunk in the same image.

Fig. 9(a) superimposes the trajectory of the robot and of the subject as recorded using the VICON stereophotogrammetric system. Despite overshooting in the path following, due to the very frequent changes in subject direction imposed by the relatively small capture volume of the stereophotogrammetric system, the robot was able to reproduce the desired path without losing the subject. The subject travelled a total path of 45.03 m, and the robot travelled 43.38 m. The norm of the distance between the subject and robot is presented in Fig. 9(b). The corresponding mean distance between the patient and robot was 1.57 ± 0.14 m. The important standard deviation value is mainly due to the starts and stops of the subject during the turning parts. Indeed, the presented data corresponded, due to the relatively small capture volume imposed by the stereophotogrammetric system, to the worst scenario in subject tracking. This value is expected to be largely smaller when walking straight.

(ii) The second experiment was designed to assess the accuracy of the proposed system in estimating the stride length. The subject was asked to walk straight in the diagonal of the capture volume. Consequently, five strides per side were recorded. The stride lengths estimated using the stereophotogrammetric system were compared with the stride lengths estimated using the proposed approach. Representative trajectories of the robot and subject are shown in Fig. 10; the corresponding distance between the robot and the subject was 1.57 ± 0.03 m. As expected, the standard deviation was lower when the robot did not have to brake and/or turn. Table 1 summarises the results for the stride length estimate. Table 1 shows the comparative results between the estimation of the stride length as estimated using the stereophotogrammetric system and the proposed system. The absolute difference between these two stride estimations, e, is lower than 0.022 m or 2% when normalised by the total stride length. Despite the few analysed strides, one can see that the method is reliable with a standard deviation of a few millimetres. These values are on the same order of magnitude compared to previous studies related to the step length

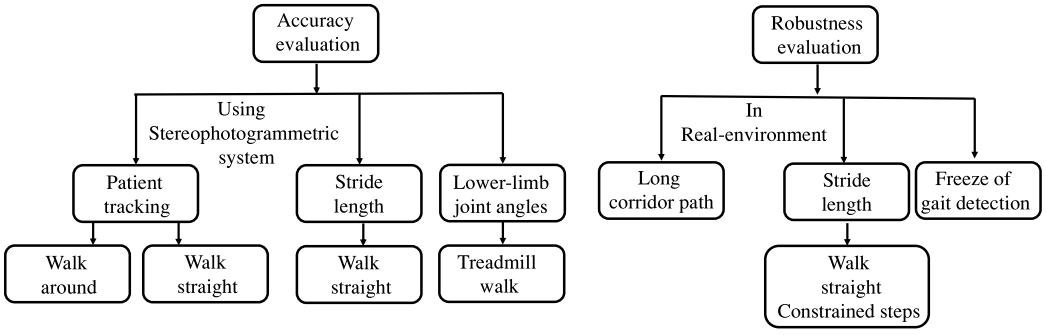

Fig. 8. Experimental procedures used for validation of the proposed system.

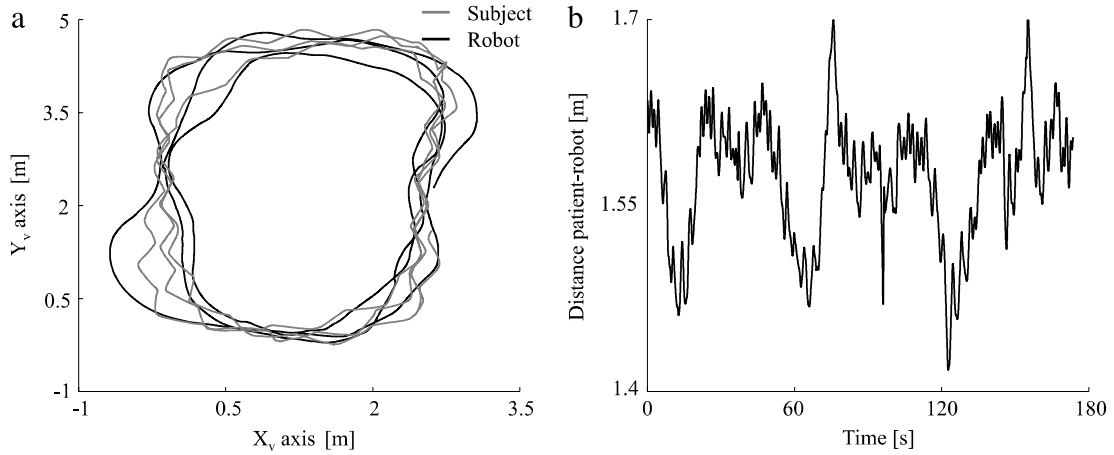

Fig. 9. Experimental results showing the robot and subject path as measured by the stereo-photogrammetric system during a square walk around the capture volume (a) and the absolute distance between the patient and robot (b).

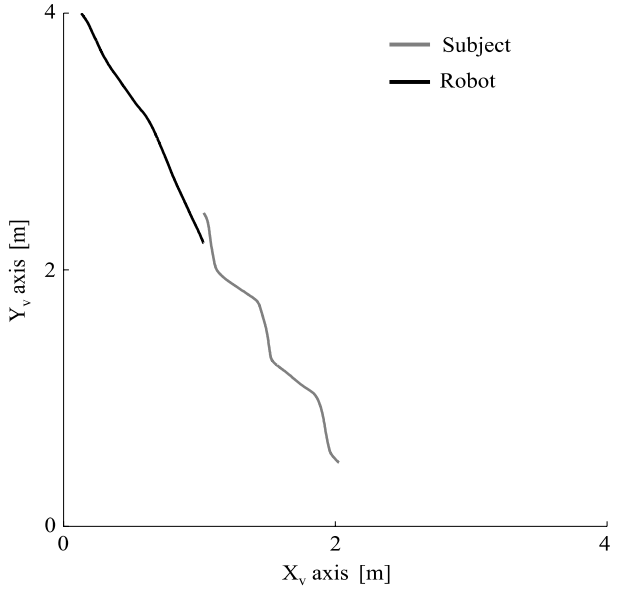

Fig. 10. Experimental results showing the robot and subject path as measured using the stereophotogrammetric system during straight walking.

estimate [4]. For example, Köse et al. recently used one IMU to estimate the step length [6] and reported an accuracy of 1.1% or 0.009 m. Their approach, despite its ease of use, is still limited to normal walking because it is strongly dependent on the signal characteristics due to the heel strike detection events and IMU signal integration. Other studies have proposed to use multiple calibrated Kinect sensors, which is similar to the stereophotogrammetric system, that implies a reduced capture volume [43]. The reported accuracy was 0.026 ± 0.024 m. In addition, this approach can result in some of the Kinect projected pattern interaction problems and may require a fine calibration phase. Finally, a reference study on Parkinson's disease [44] compares different spatio-temporal parameters with healthy subjects. The patient's average stride length was 0.96 m, while the normal walking was on average 1.31 m. This difference was superior to the accuracy of the proposed system, which could easily distinguish between the different types of walking.

(iii) The third experiment consisted of asking two volunteers (1.6 m, 50 kg, 22 years) to walk 30 s on a treadmill at their preferred velocity to simulate overground walking. Indeed, kinematic differences between overground and treadmill walking have been shown to be minimal [45]. In addition, treadmill walking was selected due to the difficulty in measuring 3D lower-limb joint angles

Table 1
Stride length error (e) obtained over 5 strides.

	e (m)	e (%)
Right	0.022 ± 0.0072	2.0
Left	0.021 ± 0.0085	1.9

Table 2
Results (mean±SD) of the comparison between the hip and knee angles (Fig. 7) as obtained using the Kinect data and the proposed inverse kinematic technique and stereophotogrammetry during treadmill walking.

		RMS (°)	CC
Hip abd/abb	Left (q_1)	2 ± 0.6	0.65
	Right (q_4)	2 ± 0.4	0.71
Hip flex/ext	Left (q_2)	4 ± 1.1	0.88
	Right (q_5)	5 ± 1.2	0.75
Knee flex/ext	Left (q_3)	8 ± 1.1	0.88
	Right (q_6)	8 ± 1.6	0.86

during straight walking over an extended period of time using the available stereophotogrammetric system. Sixteen retro-reflective markers were located on the anatomical landmarks of both legs following the marker placements as described in the Plug-in-Gait template (MX-13, VICON©). The biomechanical reference Opensim software from Stanford University [41] was used to perform the inverse kinematics of the same kinematic model described in Fig. 7.

The mean Root Mean Square (RMS) difference and Pearson's correlation coefficient (CC) between the corresponding joint angles obtained using the stereophotogrammetric system and proposed system were used to perform the accuracy analysis (Table 2). As observed from Table 2, the RMS is lower than 10° for all joints with a high correlation between the joint angles. The maximum difference is observed at the knee joint level. This is due to the large motion amplitude (mean $90° \pm 6°$).

Representative comparative results obtained from one randomly chosen trial are shown in Fig. 11. As shown in this figure, a consequential part of the RMS difference is due to the low and variable sampling frequency of the Kinect sensor and of its resampling to a constant frequency. Nevertheless, the temporal features within the joint angles estimated using the proposed approach are well respected, as are the amplitudes of the joint angles.

These preliminary results are very encouraging because they are within the range of the inter-assessor accuracy. Benedetti et al. [46] have shown that when different assessors and/or protocols are involved for gait analysis, the differences in joint angle estimations were up to 11° for the hip and 6° for the knee. In this

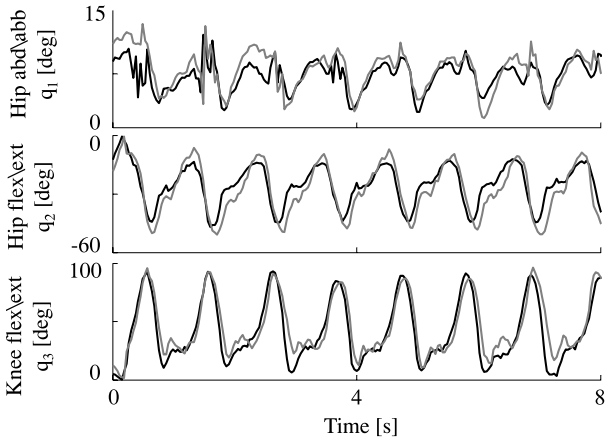

Fig. 11. Representative results obtained for the left leg joint angles for one trial: the black and grey lines indicate the joint angles calculated using the stereophotogrammetric data and Kinect data (zoom-in 8 s).

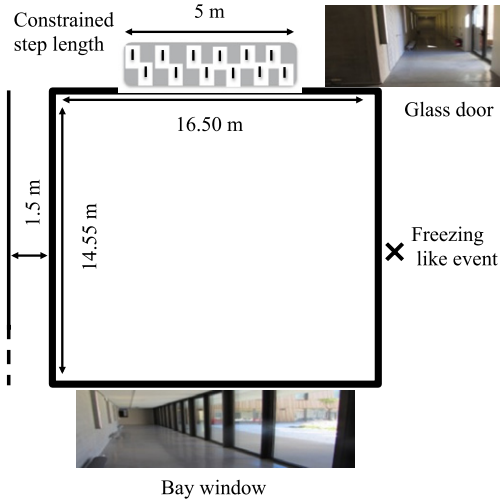

Fig. 12. Schematic view of the track used to validate the system in a real environment.

context, we believe that the proposed approach should be sufficiently accurate to assess or at least interpret the different patterns and strategies used by patients. However, an RMS error of nearly 10° will not, for example, enable the performance of satisfactory inverse dynamics for an accurate joint torque estimate [1] or quantify very accurately the small inter-subject variability observed during gait.

6.2. Field validation

To confirm the use of our system in a real environment, two experimental validations were performed. The first experiment (i) assessed the ability of the system to function under conditions similar to the clinical real environment, while the second experiment (ii) was dedicated to demonstrating the ability of the system in recovering and predicting from patient visual loss.

(i) A volunteer (1.75 m, 60 kg, 25 years) was asked to walk in a corridor and started to walk from a standing position with his heels aligned to the start line. The corridor was 1.5 m wide on average, 239 m long and consisted of four straight lines and four corners.

On one of the straight lines, a landmark on the floor indicated to the subject that he had to simulate freezing (step-in-place) for approximately 3 s. The objective was to assess the ability of the mobile robot to suddenly stop at a desired distance behind

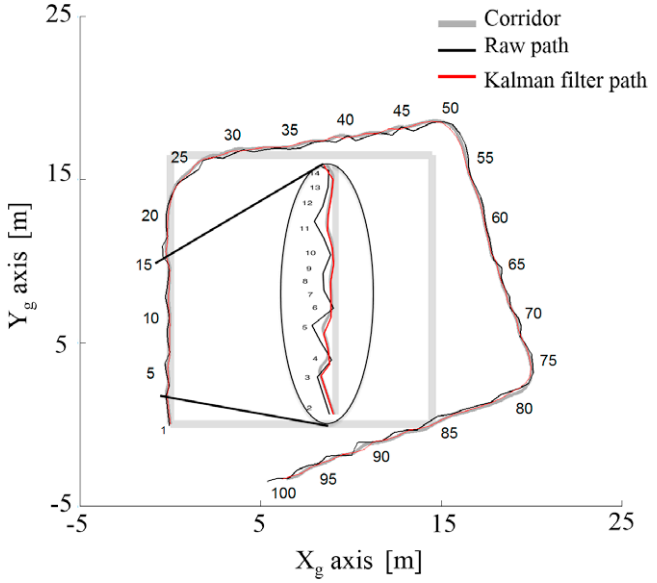

Fig. 13. Robot path during the person-following experiment in a real clinical environment. The numbers indicate the path point numbering.

the patient. A second straight line was equipped with adhesive tape, which was attached to the floor, to constrain the subject to perform a 1-m stride length for 5 m. Illumination changes were also considered to make the experiment more challenging and closer to reality. To achieve this purpose, the first straight part was performed in a corridor consisting of a bay window on one side. The other corridors were composed of neon lights and one glass door. The experimental setup is represented in Fig. 12.

The actual path of the subject, as calculated from the Kinect sensor and robot local odometry, is shown in Fig. 13. The completion of this path lasted for 300 s. As expected, due to geometrical inaccuracies such as the diameter of the wheels or sliding of the robot onto the floor, the absolute position of the patient is incorrect. This localisation problem is classical in mobile robotics and can be addressed using the Kinect sensor-based SLAM method [19]. Nevertheless, the goal of this paper was not to localise the absolute position of a patient in the laboratory but to analyse the relative (step-to-step) walking spatio-temporal parameters and these straights lines as performed in the clinical assessment. Within our framework, only straight lines, which were easy to extract from robot local odometry, would be analysed. This approach will confront eventual challenges that will be encountered while using the SLAM method in an open environment. It is also possible to imagine that the walking task will take place on a predefined path. In this case, the local odometry can be readjusted *a posteriori*.

As shown in Fig. 13, it is possible to isolate the parts where the subject was walking straight and where the robot's odometry errors are supposed to be minimal. As represented in Fig. 14, tracking of the heels and trunk of the subject can be run on these straight lines to estimate the spatio-temporal parameters.

The position of the robot along its *x*-axis (forward progression) when the patient performs the first freezing-like event (step-in-place) is shown in Fig. 15. From this figure, it is trivial to provide to the clinician an indication on the potential presence of gait freezing. The video feedback will then be essential to allow the clinicians to validate this detection. Future studies will focus on validating the detection of gait freezing based on this approach with patients who suffer from Parkinson's disease.

Table 3 summarises the results concerning the evolution of the stride length three strides before and during the constrained part of the path. Form this table, clear differences were observed between the unconstrained and constrained part of the path. The average

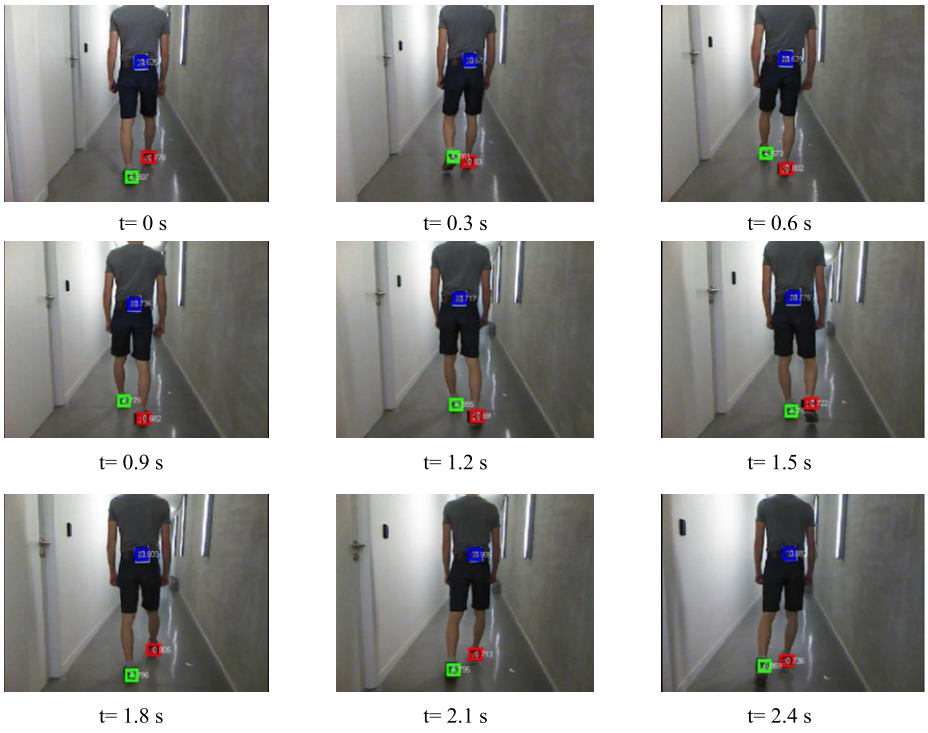

Fig. 14. Tracking of the heels and trunk of the subject using the TLD algorithm in a corridor.

Table 3

		Right side (m)	Left side (m)
Unconstrained strides	Stride-3	0.690	0.810
	Stride-2	0.782	0.726
	Stride-1	0.723	0.776
Constrained strides (1 m)	Stride 1	0.985	0.988
	Stride 2	1.015	0.961
	Stride 3	0.920	1.070
	Stride 4	0.940	0.946
	Stride 5	1.044	0.930
	Mean	0.980 ± 0.051	0.979 ± 0.055

stride lengths during the constrained part were 0.980 ± 0.051 m for the right and 0.979 ± 0.055 m for the left side. Importantly, the observed difference is a combination of the actual system error and of the inability of the subject to precisely perform a 1 m stride length. The absolute error to consider is the one calculated in Section 6.1, where the gold standard measurement was used.

(ii) To demonstrate the ability of the system to recover from subject loss, the following experimentation was performed. A volunteer was asked to walk normally when a second person was passing in between the robot and the subject to interact with the subject as in the case of a patient and their clinicians. The occlusion of the subject lasted for approximately 1.2 s. The snapshot presented in Fig. 16, which was recorded from the Kinect sensor, attests to the subject loss. The blue rectangle represents the output of the TLD tracking algorithm. As presented in Section 3.2, a Kalman filter was used to predict the trajectory of the subject up to 2 s. Fig. 17 shows the associated robot and subject trajectory as estimated using the Kalman filter.

7. Conclusions

In this study, we presented a new low-cost mobile gait analysis platform that is able to provide video feedback recorded at a constant distance and accurate stride length estimate to clinicians. The provided experimental results relative to stride length estimation

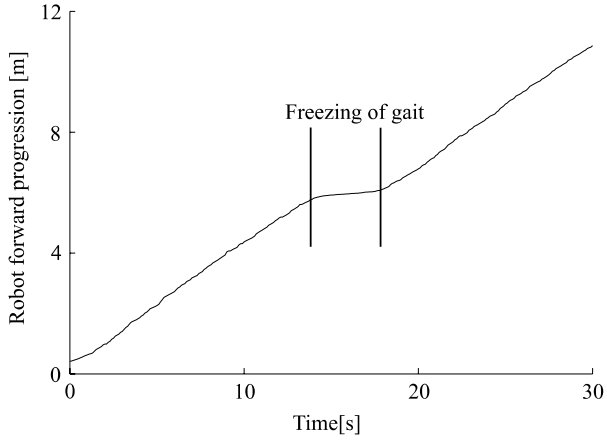

Fig. 15. Representative results showing the robot forward progression before and after the freezing-like event during straight walking.

show performances that were consistent with other methods using IMU or multiple Kinect sensors during straight walking. The accuracy of the stride length estimate, which is lower than 2.5 cm, will be sufficient in several clinical applications. However, the relatively low Kinect sensor sampling frequency will not permit the study of very small temporal variability in gait events. Nevertheless, even if this variable became popular, it is still confined to clinical research and has not, to the best of our knowledge, found a practical application in daily rehabilitation. As shown in Table 2, the presented system was able to differentiate between constrained and unconstrained stride lengths. This opens very promising perspectives in gait freezing assessment in Parkinson's disease patients. As previously discussed, due to its high variability, the detection of gait freezing is hardly achievable using only sensor data [47]. As exemplified by Fig. 15, freezing can be detected using the forward progression of the robot. However, such stops can also occur for other reasons, including door passing or a simple patient stop. In any case, the system will provide event information to the clini-

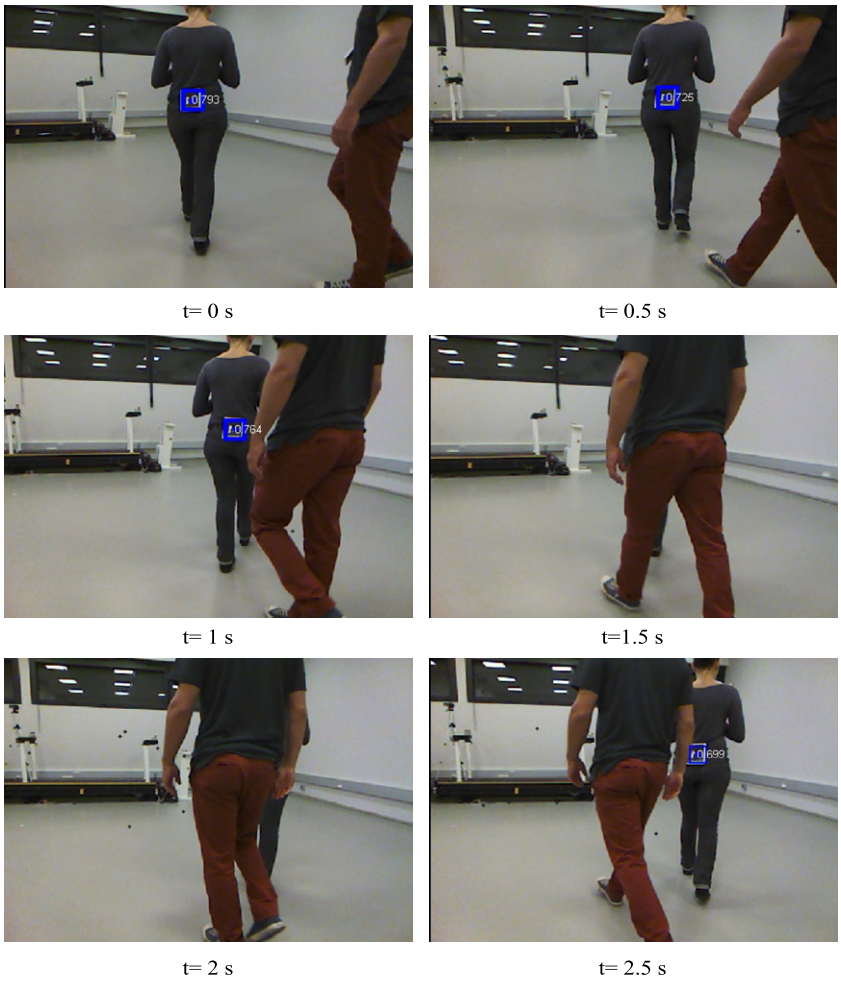

Fig. 16. Snapshot of the Kinect sensor colour camera during the experiment to demonstrate the ability of the system to recover from the subject loss. The blue rectangle represents the output of the TLD algorithm. (For interpretation of the references to colour in this figure legend, the reader is referred to the web version of this article.)

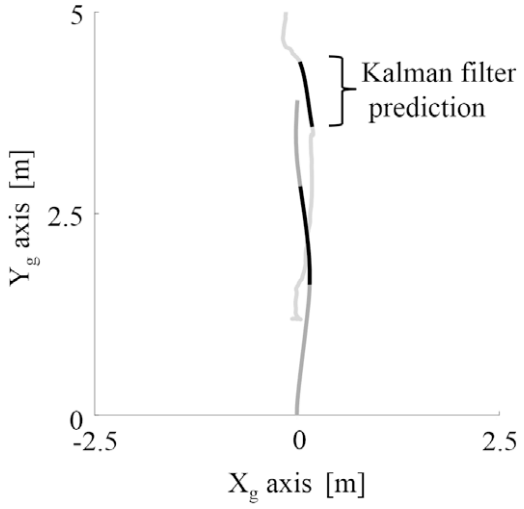

Fig. 17. Experimental results showing the subject and robot path as estimated by the proposed system. The black lines indicate the prediction of the subject motion performed using the Kalman filter during occlusion of the trunk target.

cian that is synchronised with the video timeline. The final classification of the event being made by the clinician is helped by the step length estimate and video feedback. Importantly, the system was validated in experimental conditions that were fairly similar to those that will be encountered in clinical environments. Consequently, errors collected during the real clinical assessment would be of the same order of magnitude as those presented for healthy walking. In the near future, the system will be validated over a large number of Parkinson's disease patients in a clinical centre. The threshold parameter of the step length estimate algorithm, T_h, may have to be tuned for the patient's specific walking, as is the case with any gait analysis system used for different populations. Additional gait parameters, such as medio-lateral step width, 3D trunk trajectory or gait events, can also be easily calculated using the presented system.

As experimentally shown, the retained path planning and the reactive control of the distance between the robot and subject are suitable for the indoor analysis of gait, including relatively narrow corridors. The use of the TLD algorithm in combination with depth information provided by the Kinect sensor to track a subject and his/her heels, previously equipped with targets, from a mobile robot is relevant due to its robustness and its ability to recover from subject loss. Subject loss will be unavoidable while walking in a real environment, for instance, while turning in a corridor. For this purpose, the proposed system is to use a Kalman filter to predict the subject trajectory and to help position the robot and Kinect sensor at a relevant distance for the subject.

Positioning the Kinect sensor in a vertical manner will allow a size reduction of the targets located at the trunk and heels. Additional targets could also be located on the lower limbs of the subject. Analysis of their deformations in combination with the Kinect sensor data and TLD algorithm outputs should provide accurate information regarding the 3D position of each lower-limb

segment. The preliminary results demonstrate an RMS difference that is inferior to 10° for joint angle estimates of a simplified model of the locomotor system (Fig. 7), which supports further development of a mobile low-cost human motion analysis system. At the time when this manuscript was prepared, the Kinect 2 was not available. However, announcements were made regarding the possibility of obtaining high definition of colour and depth images. This will, without a doubt, improve the global accuracy. This more accurate information will be of great help to implement the Kinect sensor-based SLAM method to improve the estimate of subject absolute position and to reduce local robot odometry errors. Future studies may also benefit from the advantage of this accuracy improvement by avoiding patterns and only directly using the amer located on the subject, i.e., clothes or skin landmark, or at least to dramatically reduce their size. Finally, a real-time estimate of the stride length may allow us to pilot more interactively auditory or visual stimuli [48] based on stride length variability. Indeed, these types of cues have been shown to have an effect on gait freezing [48].

Acknowledgements

Novartis laboratories has partially financially supported this work. The Japan Society for Promotion of Science has partially supported this work (No. PE13559). The authors would like to thank Dr. Noritaka Kawashima from the National Rehabilitation Center for Persons with Disabilities of Tokorozawa (Japan) for his help during some of the data collection.

Appendix A. Supplementary data

Supplementary material related to this article can be found online at http://dx.doi.org/10.1016/j.robot.2014.12.002.

References

[1] A. Cappozzo, Gait analysis methodology, Hum. Mov. Sci. 3 (1984) 27–50.
[2] P.L. Enright, The six-minute walk test, Respir. Care 48 (2003) 783–785.
[3] R. Baker, Measuring Walking: A Handbook of Clinical Gait Analysis, Mac Keith Press, 2013.
[4] A.M. Sabatini, C. Martelloni, S. Scapellato, F. Cavallo, Assessment of walking features from foot inertial sensing, IEEE Trans. Biomed. Eng. 52 (2005) 486–495.
[5] V. Bonnet, C. Mazzà, J. McCamley, Aurelio Cappozzo, Use of weighted Fourier linear combiner filters to estimate lower trunk 3D orientation from gyroscope sensors data, J. Neuroeng. Rehabil. 10 (2013) 29.
[6] A. Köse, A. Cereatti, U. Della Croce, Bilateral step length estimation using a single inertial measurement unit attached to the pelvis, J. Neuroeng. Rehabil. 9 (2012).
[7] S.T. Moore, D.A. Yungher, T.R. Morris, V. Dilda, H.G. MacDougall, J.M. Shine, S.L. Naismith, S.J.G. Lewis, Autonomous identification of freezing of gait in Parkinson's disease from lower-body segmental accelerometry, J. Neuroeng. Rehabil. 10 (2013).
[8] T.R. Morris, C. Cho, V. Dilda, J.M. Shine, S.L. Naismith, S.J.G. Lewis, S.T. Moore, A comparison of clinical and objective measures of freezing of gait in Parkinson's disease, Parkinsonism Rel. Disord. 5 (2012) 572–577.
[9] C. Mazzà, M. Donati, J. McCamley, P. Picerno, A. Cappozzo, An optimized Kalman filter for the estimate of trunk orientation from inertial sensors data during treadmill walking, Gait Posture 35 (2011) 138–142.
[10] D. Alvarez, R.C. Gonzalez, A. Lopez, J.C. Alvarez, Comparison of step length estimators from weareable accelerometer devices, in: Proceedings of IEEE EMBS Conference New York City, USA, 2006.
[11] J.M. Martinez-Otzeta, A. Ibarguren, A. Ansuategi, L. Susperregi, Laser based people following behaviour in an emergency environment, in: Proceedings of the International Conference on Intelligent Robotics and Applications, ICRA, 2009, pp. 33–42.
[12] Y. Motai, S.K. Jha, D. Kruse, Human tracking from a mobile agent: optical flow and Kalman filter arbitration, Signal Process., Image Commun. 27 (2012) 83–95.
[13] M. Kobilarov, G. Sukhatme, J. Hyams, P. Batavia, People tracking and following with mobile robot using an omnidirectional camera and a laser, in: Proceedings IEEE International Conference on Robotics and Automation, ICRA, 2006, pp. 557–562.
[14] Z. Jia, A. Balasuriya, S. Challa, Vision based data fusion for autonomous vehicles target tracking using interacting multiple dynamic models, Comput. Vis. Image Underst. 109 (2008) 1–21.
[15] M. Luber, L. Spinello, K.O. Arras, People tracking in RGB-D Data with on-line boosted target models, in: Proceedings of IEEE/RSJ International Conference on Intelligent Robots and Systems, IROS, 2011, pp. 3844–3849.
[16] T. Yoshimi, M. Nishiyama, T. Sonoura, H. Nakamoto, S. Tokura, H. Sato, F. Ozaki, N. Matsuhira, H. Mizoguchi, Development of a person following robot with vision based target detection, in: Proceedings of the IEEE/RSJ International Conference on Intelligent Robots and Systems, IROS, 2006, pp. 5286–5291.
[17] T. Sonoura, T. Yoshimi, M. Nishiyama, H. Nakamoto, S. Tokura, N. Matsuhira, Person following robot with vision-based and sensor fusion tracking algorithm, Comput. Vis. (2008) 519–538.
[18] Y. Salih, A.S. Malik, Comparison of stochastic filtering methods for 3D tracking, Pattern Recognit. 44 (2011) 2711–2737.
[19] J. Biswas, M. Veloso, Depth camera based localization and navigation for indoor mobile robots, in: Proceedings of IEEE International Conference on Robotics and Automation, ICRA, 2012.
[20] H. Wei Keat, B. Sunway, L.S. Ming, An investigation of the use of Kinect sensor for indoor navigation, in: Procedings of TENCON IEEE Region 10 Conference, 2012.
[21] F. Hoshino, K. Morioka, Human following robot based on control of particle distribution with integrated range sensors, in: IEEE/SICE International Symposium on System Integration, SII, 2011, pp. 212–217.
[22] W.M. Chen, S. Guo, Person following of a mobile robot using kinect through features detection based on SURF, Adv. Mater. Res. 542–543 (2012) 779–784.
[23] A. Cosgun, D.A. Florencio, H.I. Christensen, Autonomous person following for telepresence robots, in: Proceedings IEEE International Conference on Robotics and Automation, ICRA, 2013.
[24] G. Doisy, A. Jevtic, E. Lucet, Y. Edan, Adaptive person-following algorithm based on depth images and mapping, 2012.
[25] H. Zhang, L.E. Parker, 4-dimensional local spatio-temporal features for human activity recognition, in: Procedings of IEEE International Conference on Intelligent Robots and Systems, IROS, 2011, pp. 2044–2049.
[26] L. Ojeda, J.R. Rebula, P.G. Adamczyk, A.G. Kuo, Mobile platform for motion capture of locomotion over long distances, J. Biomech. 45 (2013) 2316–2319.
[27] K. Khoshelham, S.O. Elberink, Accuracy and resolution of kinect depth data for indoor mapping applications, Sensors 12 (2012) 1437–1454.
[28] C. Herrera, D. Kannala, J. Heikkilä, Joint depth and color camera calibration with distortion correction, IEEE Trans. Pattern Anal. Mach. Intell. 34 (2012) 2058–2064.
[29] J. Shotton, A. Fitgibbon, M. Cook, T. Sharp, M. Finocchio, R. Moore, A. Kipman, A. Blake, Real-time human pose recognition in parts from single depth images, Commun. ACM 56 (2013) 116–124.
[30] V. Papadourakis, A. Argyros, Comput. Vis. Image Underst. 114 (2010) 835–846.
[31] Z. Kalal, K. Mikolajczyk, J. Mata, Tracking-Learning-Detection, IEEE Trans. Pattern Anal. Mach. Intell. 6 (2010).
[32] B. Lucas, T. Kanade, Procedings of the International Joint Conference on Artificial Intelligence 81, 1981, pp. 674–679.
[33] P. Viola, M. Jones, Rapid object detection using a boosted cascade of simple features, in: International Conference on Computer Vision and Pattern Recognition, 2001.
[34] L. Lapierre, D. Soetanto, A. Pascoal, Nonsingular path following control of a unicycle in the presence of parametric modelling uncertainties, Internat. J. Robust Nonlinear Control 16 (2010) 485–503.
[35] L. Lapierre, D. Soetanto, A. Pascoal, Coordinated motion control of marine robots, in: Maneuvering Control Marine Craft IFAC Gerona, Spain, 2003.
[36] R.C. Gonzalez, R.E. Woods, S.L. Eddins, Digital Image Processing Using MATLAB, Gatesmark Publishing, 2009.
[37] C. de Boor, A Practical Guide to Splines, Springer-Verlag, 1978.
[38] S.L. Chiu, L.S. Chou, Effect of walking speed on inter-joint coordination differs between young and elderly adults, J. Biomech. 45 (2012) 275–280.
[39] A. Delval, J. Salleron, J.L. Bourriez, S. Bleuse, C. Moreau, P. Krystkowiak, L. Defebvre, P. Devos, A. Duhamel, Kinematic angular parameters in PD: reliability of joint anglecurves and comparison with healthy subjects, Gait Posture 28 (2008) 495–501.
[40] M. Morris, R. Iansek, J. McGinley, T. Matyas, F. Huxham, Three-dimensional gait biomechanics in Parkinson's disease: evidence for a centrally mediated amplitude regulation disorder, Mov. Disorders 20 (2005) 40–50.
[41] J.A. Reinbolt, A. Seth, S.L. Delp', Simulation of human movement: applications using OpenSim, in: Symposium on Human Body Dynamics, 2, 2011, pp. 186–198.
[42] M.J.D. Powell, A fast algorithm for nonlinearly constrained optimization calculations, in: G.A. Watson (Ed.), Numerical Analysis, Springer Verlag, 1978.
[43] E.E. Stone, M. Skubic, Passive in-home measurement of stride-to-stride gait variability comparing vision and kinect sensing, in: International Conference of the IEEE EMBS, Boston, 2011.
[44] M.E. Morris, R. Iansek, T.A. Matyas, J.J. Summers, Stride length regulation in Parkinson's disease. normalization strategies and underlying mechanisms, Brain 119 (1996) 551–568.
[45] P.O. Riley, G. Paolini, U. Della Croce, K.W. Paylo, D.C. Kerrigan', A kinematic and kinetic comparison of overground and treadmill walking in healthy subjects, Gait Posture 26 (2007) 17–24.
[46] M.G. Benedetti, A. Merlo, A. Leardini, Inter-laboratory consistency of gait analysis measurements, Gait Posture 38 (2013) 934–939.
[47] C. Azevedo-Coste, B. Sijobert, R. Pissard-Gobollet, M. Pasquier, B. Espiau, C. Geny, Detection of freezing of gait in Parkinson disease: preliminary results, Sensors 14 (2014) 6819–6827.

[48] S.J. Lee, J.Y. Yoo, J.S. Ryu, H.K. Park, S.J. Chung, The effects of visual and auditory cues on freezing of gait in patients with Parkinson disease, Am. J. Phys. Med. Rehabil. 91 (2012) 2–11.

Vincent Bonnet received the B.E. degree in Electrical Engineering, in 2005, and the Ph.D. degree in Automatics Control and Robotics, in 2009, both from the science University of Montpellier 2. From 2010 to 2012, he was working as a post-doc in Rome, Italy under the direction of Professor Aurelio Cappozzo. In 2013 he was teaching assistant at the University of Montpellier-Euromov Institute and he is now working at the University of Tokyo Agriculture and Technology in Tokyo, Japan. His research interests include various aspects of low-cost sensors, motion analysis, humanoid robotics, system identification and control.

Christine Azevedo-Coste received the M.S. degree from the National Polytechnic Institute of Grenoble, Grenoble, France, and the Ph.D. degree from INRIA Rhone-Alpes, Grenoble, France, in 1999 and 2002, respectively. From 2002 to 2003, she was a Postdoctoral Fellow at INPC, France. From 2003 to 2004, she was a Guest Researcher at the SMI Center, Denmark. Since 2004, she has been a Researcher with INRIA Sophia Antipolis and Laboratoire d'Informatique, de Robotique et de Microélectronique de Montpellier (LIRMM), DEMAR team, Montpellier, France. Her research interests include movement control, functional rehabilitation and assistive devices mainly involving electrical stimulation.

Lionel Lapierre received his Ph.D. degree in Robotics, from the University of Montpellier 2, Montpellier, France, in 1999. Then, he joined the team of Professor A. Pascoal within the European project FreeSub for three years. Since 2003, he has been with the Underwater Robotics Division, Laboratoire d'Informatique, de Robotique et de Microélectronique de Montpellier (LIRMM), Montpellier, France. He is now working with the Lab team EXPLORE, leading the REEA project.

Jean Maximilien Cadic is a student in Artificial Intelligence at the UPMC (Sorbonne University). He received a B.S. in Mathematics and a B.A. in Sociology from the University Montpellier 2 and University Montpellier 3. His research interests include ambient intelligence, group dynamics and human–robot interaction.

Philippe Fraisse is currently Professor at the Université Montpellier 2 (LIRMM, Laboratory), France. He received the Master of Electrical Engineering of Ecole Normale Supérieure de Cachan in 1988. He received Ph.D. degree in Automatic Control of Université Montpellier 2 on position/force control dor two-arm robots, France, in 1994. His research interests include human–robot interaction, humanoid robotics, robotics for rehabilitation and mobile manipulators. He is involved in the Japanese–French Joint Laboratory for Robotics (AIST-CNRS JRL) based in Tsukuba, Japan.

René Zapata is a researcher at the University of Montpellier in the Laboratory of Robotics, Computer Science and Microelectronics (LIRMM). His fields of interest are Robot Control, Robots Dynamics, Collision Avoidance and Localization for ground mobile robots, flying robots and underseas robots. He teaches linear control, advanced control and mobile robotics in the Master track and at the Engineering School Polytech Montpellier. He is the head of the EXPLORE project in charge of developing tools and algorithms for environment exploration robots.

Gentiane Venture has completed an Engineer's degree from the Ecole Centrale of Nantes (France) in 2000 in Robotics and Automation and a M.Sc. from the University of Nantes (France) in Robotics. In 2003, she obtained her Ph.D. from the University of Nantes (France). In 2004 she joined the French Nuclear Agency (Paris, France). Later she joined Prof. Yoshihiko Nakamura's Lab. at the University of Tokyo (Japan) with the support of the JSPS. In March 2009, she becomes an Associate Professor and starts a new lab at the Tokyo University of Agriculture and Technology (Japan). Her main research interests include: Non-verbal communication, Human behaviour understanding from motion, Human body dynamics modelling, Dynamics identification, Control of robot for human/robot interaction, Human affect recognition.

Christian Geny received the M.D. degree from the University of Grenoble, France in 1988. He had a fellowship in 1991 to 1994 in the Inserm U421. From 2002 to 2004, he served as a head of department of neurology at François Mitterrand Hospital, Pau, France. Since 2004, he joined University Hospital of Montpellier as consulting neurologist in the Departments of Neurology and Geriatrics. He is member of the research team M2H (Movement to Health, Montpellier, France). His research interests include Parkinson disease, tremor and cognitive aspects of locomotion. He is actually head of Parkinson Disease Unit of Montpellier from 2013.